Wave Synchronizing Crane Control during Water Entry in Offshore Moonpool Operations

Svein I. Sagatun[1], Tor A. Johansen[2], Thor I. Fossen[2], and Finn G. Nielsen[1]

Abstract

A new strategy for active control in heavy-lift offshore crane operations is suggested, by introducing a new concept referred to as wave synchronization. Wave synchronization reduces the hydrodynamic forces by minimization of variations in the relative vertical velocity between payload and water using a wave amplitude measurement. Wave synchronization is combined with conventional heave compensation to obtain accurate control. Experimental results using a scale model of a semi-submerged vessel with a crane and moonpool shows that wave synchronization leads to significant improvements in performance. Depending on the sea state and payload, the results indicate that the reduction in the standard deviation of the wire tension may be up to 50 %.

1 Introduction

Higher operability of installations offshore of underwater equipment will become increasingly more important in the years to come. Offshore oil and gas fields will be developed with all processing equipment on the seabed and in the production well itself. Norsk Hydro has already one year of operational experience with the Troll Pilot subsea oil processing plant. This subsea plant is made up of a three phase subsea separator, a 1.6 MW electrical single phase pump and a reinjection tree; everything located on 320 m water depth outside the west coast of Norway. The lower cost in using subsea equipment compared to using a floating or fixed production platform is penalized with lower availability for maintenance, repair and replacement of equipment. Production stops due to component failure is costly, hence a high operability on subsea intervention is required to operate subsea fields. High operability implies that subsea intervention must be carried out also during winter time, which in the North Sea and other exposed areas implies underwater intervention in harsh weather conditions.

Standard industrial heave compensation systems applied to offshore cranes or module handling systems (MHS) have been used by the industry for years, see for instance [1, 2, 3, 4, 5] and references therein. These systems normally work with acceleration feedback or feedforward, where the vertical acceleration is measured on the vessel, on the crane boom, or MHS structure. Alternatively, a passive spring-damper mechanism together with position control of the crane hook is used for heave compensation.

This article focuses on active control of heave compensated cranes or MHS during the *water entry phase* of a subsea installation or intervention. We assume that the payload is launched through a moonpool from a typical mono hull installation vessel. During the water entry phase the hydrodynamic loads due to waves within the moonpool may be significant, and not directly accounted for in a heave compensation system. The main contribution of the present work is the use of moonpool wave amplitude feedforward control in order to achieve wave synchronized motion of the payload through the water entry zone. We believe this concept is new.

[1]Norsk Hydro Exploration and Production, Bergen, Norway. Svein.Ivar.Sagatun@hydro.com, Finn.Gunnar.Nielsen@hydro.com

[2]Department of Engineering Cybernetics, Norwegian University of Science and Technology, N-7491, Trondheim, Norway. Tor.Arne.Johansen@itk.ntnu.no, tif@itk.ntnu.no

2 Mathematical modelling

We will only consider the vertical motion of a payload moving through the water entry zone, handled from a floating vessel. It is assumed that the vessel is kept in a mean fixed position and heading relative to the incoming wave. Effects from the vessel's roll and pitch motion are neglected.

2.1 Dynamics of scale model crane-vessel

In this section we describe the rigid-body dynamics of a laboratory scale model moonpool crane-vessel (scale 1:30), see Figures 1 and 2 of a setup consisting of an electric motor and a payload connected by a wire that runs over a pulley suspended in a spring. The spring is designed to simulate a realistic wire elasticity in the scale model. We remark that this setup contains no passive heave compensation system.

The equations of motion for the motor and payload are

$$m_m \ddot{z}_m = F_m + F_t \quad (1)$$

$$m(\ddot{z} + \ddot{z}_0) = mg + f_z - F_t \quad (2)$$

where $z_m = R\theta_m$, $m_m = J_m/R$, $F_m = T_m/R$, and

θ_m	=	motor angle (rad)
R	=	radius of the pulley on the motor shaft (m)
J_m	=	motor inertia (kg/m)
T_m	=	motor torque (Nm)
m	=	payload mass (kg)
z_0	=	vessel position in heave (m)
z	=	payload position (m)
z_m	=	motor position (m)
ζ	=	wave amplitude at center of moonpool (m)
F_t	=	wire tension (N)
f_z	=	hydrodynamic and static force on payload (N)

All vertical coordinate systems and forces are positive downwards. The coordinate systems of z, z_m and z_p are fixed in the vessel, while the coordinate systems of ζ and z_0 are Earth-fixed, see Figure 2. All have the origin at the still water mean sea level.

The wire runs over a pulley suspended in a spring. The mass moving with the pulley is denoted m_p, and the vertical position of the pulley is z_p. The equation of motion for the pulley is:

$$m_p \ddot{z}_p + d_p \dot{z}_p + k_p z_p = F_t \quad (3)$$

where d_p is the damping coefficient and k_p the spring coeffecient. Substitution of $z = z_m + z_p$ into (3) gives the following expression for the wire force

$$F_t = m_p(\ddot{z} - \ddot{z}_m) + d_p(\dot{z} - \dot{z}_m) + k_p(z - z_m) \quad (4)$$

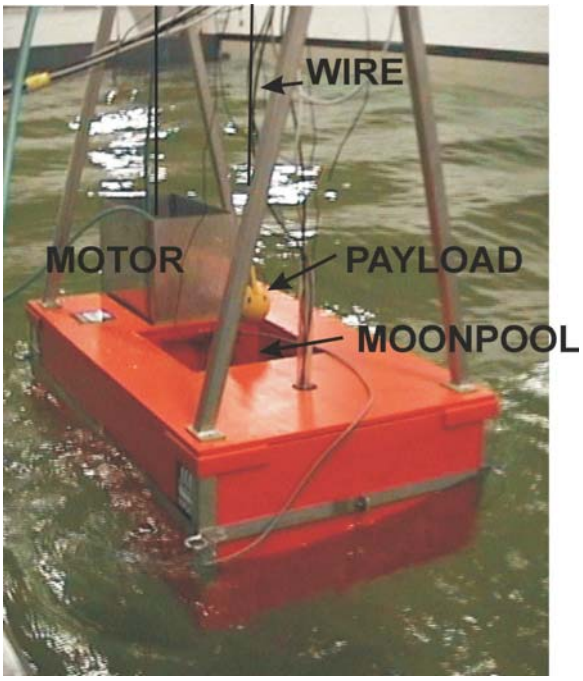

Figure 1: Rig-crane scale model.

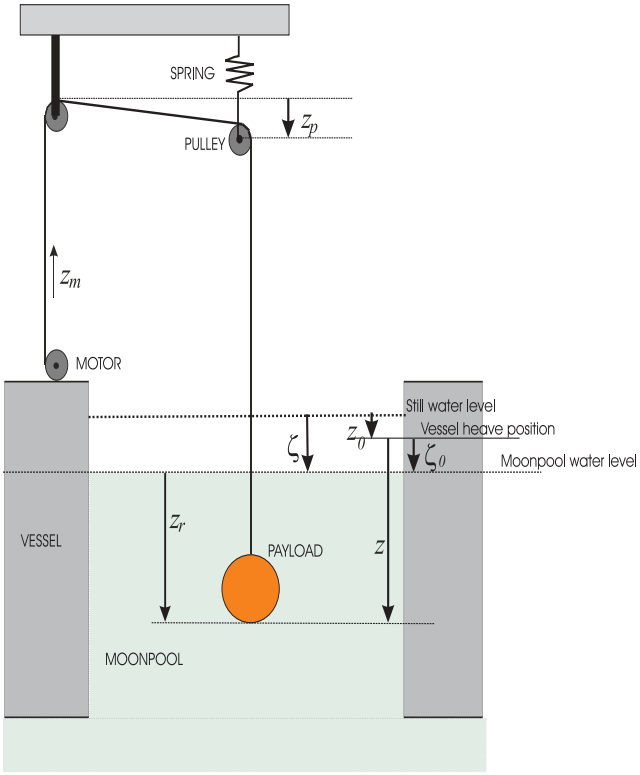

Figure 2: Definition of the coordinate systems.

2.2 Loads and load effects

The hydrodynamics in this section is based on [6, 7] and references therein. Let z_r denote the vertical position of the payload relative to the wave surface elevation ζ in the center of the moonpool, with $z_r > 0$ when the payload is submerged, see Figure 2. The vertical hydrodynamic load on a payload going through the water entry zone may be expressed as the sum of forces from potential theory f_{zp} and viscous forces f_{zv}. The force f_{zp} may be expressed as follows:

$$\begin{aligned} f_{zp} &= -\rho g \nabla(z_r) - \rho \nabla(z_r) \frac{d}{dt}\frac{\partial \phi}{\partial z}\bigg|_z \\ &\quad + \frac{d}{dt}\left[Z_{\dot{z}_r}(z_r)\left(\frac{dz}{dt} - \frac{\partial \phi}{\partial z}\right)\right] \end{aligned} \tag{5}$$

The term $\nabla(z_r)$ represents the instantaneous submerged volume and ϕ is the scalar wave velocity potential function defined such that $\frac{\partial \phi}{\partial z}$ and $\frac{d}{dt}\frac{\partial \phi}{\partial z}$ become the wave velocity and acceleration in the z-direction respectively. The term $Z_{\dot{z}_r}(z_r)$ is the (position depended) added mass of the product in the z-direction. The second term on the right hand side of (5) represents Froude-Kriloff pressure forces and is by definition only depended of the velocity of the water particles. The velocity potential may for infinite water depth be written as:

$$\phi = \frac{g\zeta_a}{\omega} e^{-kz} \cos(\omega t - kx) \tag{6}$$

where the wave number k and the wave profile $\zeta(t)$ is defined as $k = \omega^2/g$ and $\zeta(t) = \zeta_a \sin(\omega t - kx)$. ω and ζ_a denote the wave frequency and amplitude respectively. The time varying sea surface elevation can be represented as a sum of a large number of wave components, thus

$$\zeta(t) = \sum_{j=1}^{N} A_j \sin(\omega_j t - k_j x + \varepsilon_j) \tag{7}$$

where A_j and ε_j are the Fourier amplitude and the constant random phase for the j'the wave component. Notice that (5) only consider loads derived based on potential theory. We will also have a viscous drag on the submerged product on the form

$$f_{zv} = -\frac{1}{2}\rho C_D A_{pz} \dot{z}_r \left|\dot{z}_r\right| - d_l \dot{z}_r \tag{8}$$

where C_D is the drag coefficient and A_{pz} is the projected efficient drag area in the vertical direction. The force $d_l \dot{z}_r$ represents the linear drag. Hence the hydrodynamic and static forces acting on the object become:

$$\begin{aligned} f_z &= -\rho g \nabla(z_r) - \rho \nabla(z_r)\ddot{z} - Z_{\ddot{z}_r}(z)\ddot{z}_r \\ &\quad - \frac{\partial Z_{\dot{z}_r}(z_r)}{\partial z_r}\dot{z}_r^2 - \frac{1}{2}\rho C_D A_{pz}\dot{z}_r\left|\dot{z}_r\right| - d_l\dot{z}_r \end{aligned} \tag{9}$$

Notice that the impulsive hydrodynamic slamming loads generated when waves hit the product represented by $\frac{\partial Z_{\dot{z}_r}}{\partial z_r}\dot{z}_r^2$ is directed upward since $\frac{\partial Z_{\dot{z}_r}}{\partial z_r} > 0$.

We refer to [8] Part 2 chapter 6 and [9] for rules and regulations and more detailed mathematical modelling of the water entry problem. Equation (7) refer to the wave elevation for undisturbed sea. Resonance oscillations of the wave elevation may occur in the moonpool. The linearized wave

elevation dynamics in the moonpool may be formulated as follows, [6]:

$$\frac{d^2\zeta}{dt^2} + d_m\dot{\zeta} + \frac{g}{h_m}\zeta = -\frac{1}{h_m}\frac{\partial\phi(\zeta)}{\partial t} \tag{10}$$

where h_m is the still water depth of the moonpool with constant circular cross section. Notice that the moonpool's natural frequency is $\omega_m = \sqrt{g/h_m}$. This is in the same range as the significant wave frequencies, thus resonance behavior will occur. The linearized damping parameter d_m may be set to $d_m = \frac{d_{mq}}{h_m}\sqrt{8/\pi}\sigma_{\dot{\zeta}}$ where $d_{mq} = \frac{1}{2}\rho C_{Dm} A_m$ and $\sigma_{\dot{\zeta}}$ is the standard deviation of the velocity of the wave elevation in the moonpool, [10] pp. 303-307. C_{Dm} and A_m are the drag coefficient and the characteristic drag area in the moonpool respectively.

2.3 Experimental setup and instrumentation

The total scale model mass is 157 kg with a water plane area of 0.63 m^2 and moonpool depth $h_m = 0.29$ m. Further details can be found in [11, 12]. We consider several payloads, including a sphere, a cylinder and a pump mounted inside an open frame. The standard payload is a sphere with diameter 0.09 m and mass 0.582 kg. In full scale, this corresponds to a payload diameter of 2.7 m with mass 15.85 tons. The winch motor is an AC servomotor with an internal speed control loop. There are vertical accelerometers in both the payload and vessel, and a wire tension sensor. In the moonpool there are wave meters measuring the wave amplitude in a vessel-fixed coordinate frame, i.e. $\zeta_0(t) = \zeta(0,t) - z_0(t)$. The motor position z_m is measured using an encoder.

3 Frequency analysis

When the payload is partly or fully submerged, the hydrodynamic force f_z given by (9) influences the wire/suspension resonance frequency. This leads to increased damping and effects of added mass and its time-derivative. Depending on parameters such as the size, shape, mass, position and velocity of the payload, a significant reduction in the resonance frequency and increase in the relative damping factor is experienced, compared to motion in air. 48.8 rad/s is the experimentally determined wire resonance frequency with the spherical payload with mass of 0.572 kg, when the payload is moving in air, [13]. Typical values with the payload in submerged condition are 31 rad/s to 46 rad/s, [13].

The frequency-dependent ratio between wave amplitudes inside the moonpool and in the basin is illustrated in Figure 3. The data are experimental and based on a frequency-sweep using regular waves at 2 cm amplitude. We notice the characteristic resonance near the period $T_m = 1.3$ s, or $\omega_m = 4.83$ rad/s, see also [14].

Typical vessel heave frequencies are in the range $4.0 \leq \omega_{heave} \leq 9.0$ rad/s. The natural frequency of the heave motion of the vessel was found experimentally to be approximately $\omega_{heave} = 4.8$ rad/s, see also [14, 15].

A first order model of the transfer function from the reference speed $\dot{z}_d$ to the motor speed $\dot{z}_m$ is

$$\frac{\dot{z}_m}{\dot{z}_d}(s) = \frac{e^{-0.010s}}{1 + 0.020s} \tag{11}$$

The time-delay is mainly due to digital communication between the motor drive and control units. At $\omega = 6.3$ rad/s the motor gives a phase loss of approximately 12 deg.

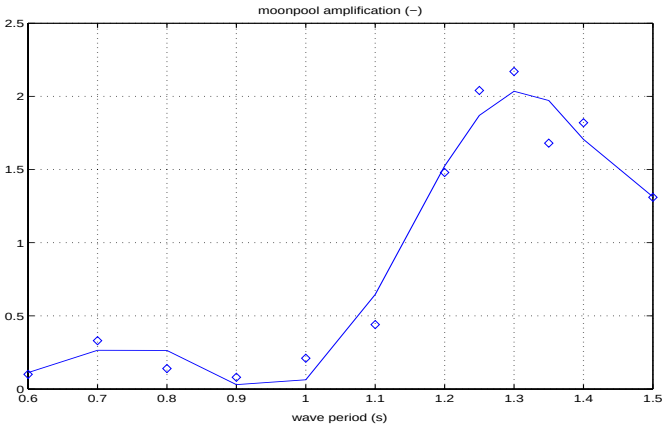

Figure 3: Ratio between wave amplitudes in moonpool and basin as a function of basin wave period (least squares curve fit). Notice the resonance at $T_m = 1.3$ s.

4 Compensator strategies

We focus on feedforward compensator strategies, since the main disturbances can be estimated reliably from measurements, and the wire/suspension elasticity introduces resonances that give fundamental limitations to the achievable feedback control bandwidth. The main performance measures of interest are the wire tension and hydrodynamic forces on the payload. The minimum value must never be less than zero to avoid high snatch loads, and the peak values and variance should be minimized.

4.1 Active heave compensation

The objective of a heave compensator is to make the payload track a given trajectory in an Earth-fixed vertical reference system. This means that the payload motion will not be influenced by the heave motion of the vessel. This is implemented using feed-forward where an estimate $\hat{\dot{z}}_0$ of the vessel's vertical velocity (in an Earth-fixed vertical reference system) is added to the motor speed reference signal $\dot{z}_m^*$ commanded by the operator or a higher level control system:

$$\dot{z}_d \quad = \quad \dot{z}_m^* + \hat{\dot{z}}_0 \tag{12}$$

The vessel vertical velocity $\dot{z}_0$ can be estimated using an estimator which essentially integrates an accelerometer signal and removes bias using a high-pass filter because it can be assumed that the vessel oscillates vertically around zero Earth-fixed position (mean sea level):

$$\hat{\dot{z}}_0(s) \quad = \quad \frac{H_{hp}(s)}{s}\ddot{z}_0(s) \tag{13}$$

where $\ddot{z}_0$ is the measured vessel acceleration and $H_{hp}(s)$ is a 2nd order high-pass filter with cutoff frequency below the significant wave frequencies:

$$H_{hp}(s) \quad = \quad \frac{s^2}{\omega_c^2 + 2\cdot 0.45\cdot\omega_c s + s^2} \tag{14}$$

with cutoff frequency $\omega_c = 1.37$ rad/s, well below significant wave frequencies.

4.2 Wave synchronization

Wave amplitude measurements can be used in a feed-forward compensator to ensure that the payload motion is synchronized with the water motion during the water entry phase. An objective is to minimize variations in the hydrodynamic forces on the payload, $|f_{zd}(z_r)|$, where

$$\begin{aligned} f_{zd} &= -\rho\nabla(z_r)\ddot{z} - Z_{\ddot{z}_r}(z_r)\ddot{z}_r - \frac{\partial Z_{\dot{z}_r}(z_r)}{\partial z_r}\dot{z}_r^2 \\ &\quad -\frac{1}{2}\rho C_D A_{pz}\dot{z}_r\left|\dot{z}_r\right| - d_l\dot{z}_r \end{aligned} \tag{15}$$

This equation represents the dynamic part of (9). The first term of (15) is the Froude-Kriloff pressure force. The second term represents the contribution of the added mass, while the third term contains the slamming loads. The fourth term is the viscous drag on the payload. Rather than minimizing this expression explicitly, we observe that a close to optimal solution is achieved by minimizing variations in $\dot{z}_r$, the relative vertical velocity of the payload and water. Since

$$z_r = z - \zeta_0 \tag{16}$$

we get the approximation $\dot{z}_r \approx \dot{z} - \dot{\zeta}_0\kappa(z)$ by assuming that the wave amplitude decays with depth according to the function $\kappa(z)$. Hence, wave synchronization is achieved by the feed-forward compensator

$$\dot{z}_d = \dot{z}_m^* + \dot{\hat{\zeta}}_0\kappa(z) \tag{17}$$

where $\dot{\hat{\zeta}}_0$ is an estimate of the velocity of the wave surface elevation inside the moonpool (in a vessel-fixed coordinate frame). The factor $\kappa(z)$ accounts for the dependence of the water vertical velocity on water depth. Since the moonpool operates as a piston in a cylinder, the water vertical velocity may be assumed to be constant from the wave surface to the bottom of the moonpool, and decay exponentially below this point:

$$\kappa(z) = \begin{cases} 1, & z \le h_m \\ \exp(-k(z-h_m)), & z > h_m \end{cases} \tag{18}$$

Since this control should only be applied during the water entry phase, we introduce the factor $\alpha(z)$ and blends the wave synchronization with heave compensation:

$$\dot{z}_d = \dot{z}_m^* + \dot{\hat{\zeta}}_0\alpha(z)\kappa(z) + \dot{\hat{z}}_0(1-\alpha(z)\kappa(z)) \tag{19}$$

The position-dependent factor $\alpha(z)$ goes smoothly from zero to one when the payload is being submerged, for example

$$\alpha(z) = \begin{cases} 0, & z < -0.10 \\ 10(z+0.10), & -0.10 \le z \le 0 \\ 1, & z > 0 \end{cases} \tag{20}$$

The feedforward (19) contains both wave synchronization and heave compensation, and when z is large this expression coincides with the heave compensator (12). Also notice that when the water inside the moonpool does not move ($\zeta = 0$, which gives $\zeta_0 = -z_0$) the wave synchronization (19) also coincides with the heave compensator (12) for all z.

The wave amplitude ζ_0 relative to a vessel-fixed position inside the moonpool is measured. The wave amplitude velocity $\dot{\zeta}_0$ is estimated by filtering and (numerical) differentiation:

$$\dot{\hat{\zeta}}_0(s) = sH_{lp}(s)H_{notch}(s)\zeta_0(s) \tag{21}$$

The low pass filter $H_{lp}(s)$ is composed of a 2nd order critically damped filter at 60 rad/s and a 2nd order critically damped filter at 200 rad/s. In order to avoid exciting the wire resonance, we have introduced a notch filter

$$H_{notch}(s) = \frac{s^2 + 2\cdot 0.1\cdot\omega_n + \omega_n^2}{s^2 + 2\cdot 0.5\cdot\omega_n + \omega_n^2} \tag{22}$$

typically tuned at $\omega_n \approx \omega_3$. In the experiments we used $\omega_n = 37$ rad/s.

5 Experimental results

In this section we summarize experimental results with the heave compensation and wave synchronization control strategies described above. More data and results with several payloads in regular and irregular waves can be found in [12]. The experiments were carried out in the MCLab [16] at NTNU.

The two scenarios we present here represent typical performance improvements that can be achieved:

- **Spherical payload in regular waves with period $T = 1.25$ s and amplitude $A = 1.8$ cm**. This wave frequency is close to the moonpool resonance frequency, see Figure 3, and the wave amplitude inside the moonpool is about 2 times the basin wave amplitude. The equivalent wave height in full scale is around $H_s = 1.1$ m and the period is 6.8 s.

- **Spherical payload in regular waves with period $T = 1.0$ s and amplitude $A = 6.8$ cm.** At this frequency there is no resonance. The equivalent wave height in full scale is around $H_s = 4.1$ m and the period is 5.5 s.

We present both raw and filtered wire tension data. The filtered data contains mainly components in the frequency band between 3.1 rad/s and 9.4 rad/s, where the significant wave motion is located (the filtering is carried out using 4th order filters with no phase shift). This filtering allows the effects of the wave synchronization to be separated from other effects, since this is the frequency band where the wave synchronization is effective. It is therefore natural to verify the performance of the wave synchronization on the filtered data, neglecting low-frequency components due to buoyancy and high-frequency components due to measurement noise and wire/suspension resonances. Still, it is also of interest to evaluate the performance of the wave synchronization with respect to excitation of the wire/suspension resonance. This evaluation is, however, not straightforward to carry out since the laboratory model does not contain passive heave compensation or damping. Moreover, the excitations caused by signal noise and winch motor drive are not directly scalable to a full scale implementation and must be considered in the context of the technology used for implementation. Thus, we will base our conclusions mainly on the filtered data.

5.1 Regular waves at $T = 1.25$ s and $A = 1.8$ cm

Figure 4 shows the wire tension for test series B (two tests A and B are carried out at each sea state to verify repeatability) with the spherical payload, with and without control. The following observations and remarks can be made:

- The wave synchronization reduces the tension standard deviation by 25.2 % in test A and 21.4 % in test B, compared to no control, when considering filtered data. Wave synchronization in combination with heave compensation reduces the tension standard deviation by 22.0 % in test A and 21.8 % in test B, compared to no control, when considering filtered data.
- The use of heave compensation does not give any significant reduction of tension variability in this sea state. However, it gives significant reduction of the standard deviation of the payload acceleration. The reason for this is that the heave motion is fairly small compared to the resonant moonpool water motion.
- When considering the unfiltered data, similar qualitative conclusions can be made.

5.2 Regular waves at $T = 1.0$ s and $A = 6.8$ cm

Figure 5 shows the wire tension for test series B with the spherical payload, with and without control. We make the following observations and remarks:

- The wave synchronization reduces the tension standard deviation by 31.0 % in test A and 33.1 % in test B, compared to no control, when considering filtered data. Wave synchronization in combination with heave compensation reduces the tension standard deviation by 48.1 % in test A and 54.2 % in test B, compared to no control, when considering filtered data.
- The use of heave compensation alone gives significant reduction of tension variability in this very rough sea state, namely 50.3 % in test A and 25.9 % in test B. This indicates that significant reduction in tension variance can be achieved by either heave compensation or wave synchronization, but largest reduction is achieved by combining them.
- When considering the unfiltered data, similar qualitative conclusions can be made in most cases.

6 Discussion and conclusions

Wave synchronization, either alone or in combination with heave compensation, significantly reduces wire tension variability and peak values in a large majority of the tests. However, under some sea states and for some payloads, no or only small improvement was experienced. The experiments with regular waves showed good repeatability, giving consistent conclusions with different experiments under the same sea state.

The feedforward approach leads to a phase error, due to the dynamics of the motor and signal filtering. In our experimental setup this error is significant, and not compensated for. For a wave period of 1.0 s, the phase loss in the motor is 12 degrees and the phase loss in the filtering of the wave amplitude measurement is about 25 deg. The total phase loss is around 37 deg. It is therefore clear that the use of some model-based predictor of the wave amplitude may lead to significant improvement of performance.

Acknowledgements

The authors are grateful to Marintek for kind assistance during the experiments.

References

[1] NSLT, *The 5th North Sea Offshore Crane Conference, Aberdeen, Scotland*, Norwegian Society of Lifting Technology (NSLT), 2000.

[2] NSLT, *Underwater Lifting Operations, Stavanger, Norway (in Norwegian)*, Norwegian Society of Lifting Technology (NSLT), 2000.

[3] NSLT, *The 3th International Offshore Crane Conference, Kristiansand, Norway*, Norwegian Society of Lifting Technology (NSLT), 1998.

[4] S. I. Sagatun, T. I. Fossen, and K. P. Lindegaard, "Inertance control of underwater installations," in *Preprint IFAC CAMS, Glasgow, Scotland*, 2001.

[5] U. A. Korde, "Active heave compensation on drillships in irregular waves," *Ocean Engineering*, vol. 25, pp. 541–561, 1998.

[6] O. M. Faltinsen, *Sea Loads on Ships and Offshore Structures*, Cambridge University Press, New York, 1990.

[7] J. N. Newman, *Marine Hydrodynamics*, Cambridge, MA: MIT Press, 1977.

[8] DnV, *Rules for Planning and Execution of Marine Operations*, DnV, Norway, 2000.

[9] M. Greenhow and L. Yanbao, "Added masses for circular cylinders near or penetrating fluid boundaries - review, extension and application to water-entry, -exit and slamming," *J. Ocean Engineering*, vol. 14, pp. 325–348, 1987.

[10] W. Price and R. Bishop, *Probabilistic Theory of Ship Dynamics*, London, UK: Chapman and Hall, 1974.

[11] T. I. Fossen and T. A. Johansen, "Modelling and identification of offshore crane-rig system," Tech. Rep. 2001-12-T, http://www.itk.ntnu.no/research/-HydroLab/reports/hydrolaunch_model.pdf, Department of Engineering Cybernetics, NTNU, Trondheim, Norway, 2001.

[12] T. A. Johansen and T. I. Fossen, "Observer and controller design for an offshore crane moonpool system," Tech. Rep. 2001-13-T, http://www.itk.ntnu.no/research/-HydroLab/reports/hydrolaunch_control.pdf, Department of Engineering Cybernetics, NTNU, Trondheim, Norway, 2001.

[13] T. A. Johansen and T. I. Fossen, "HydroLaunch free decay tests," Tech. Rep. 2001-18-T, http://www.itk.ntnu.no/-research/HydroLab/reports/hydrolaunch_free_decay.pdf, Department of Engineering Cybernetics, NTNU, Trondheim, Norway, 2001.

[14] F. G. Nielsen, "Coupled hydrodynamics for the HydroLaunch vessel with load," Working note, Norsk Hydro, Exploration and Production, Bergen, Norway, http://www.itk.ntnu.no/research/HydroLab/reports/-HydroLab_dynamics.pdf, 2002.

[15] M. P. Fard and F. G. Nielsen, "Simulation of coupled vessel-load dynamics," Tech. Rep. NH-00036960, http://www.itk.ntnu.no/research/HydroLab/-reports/Fard2002.pdf, Norsk Hydro, Exploration and Production, Bergen, Norway, 2001.

[16] "MCLab - Marine Cybernetcs Laboratory, Trondheim," http://www.itk.ntnu.no/marinkyb/MCLab/, 2002.

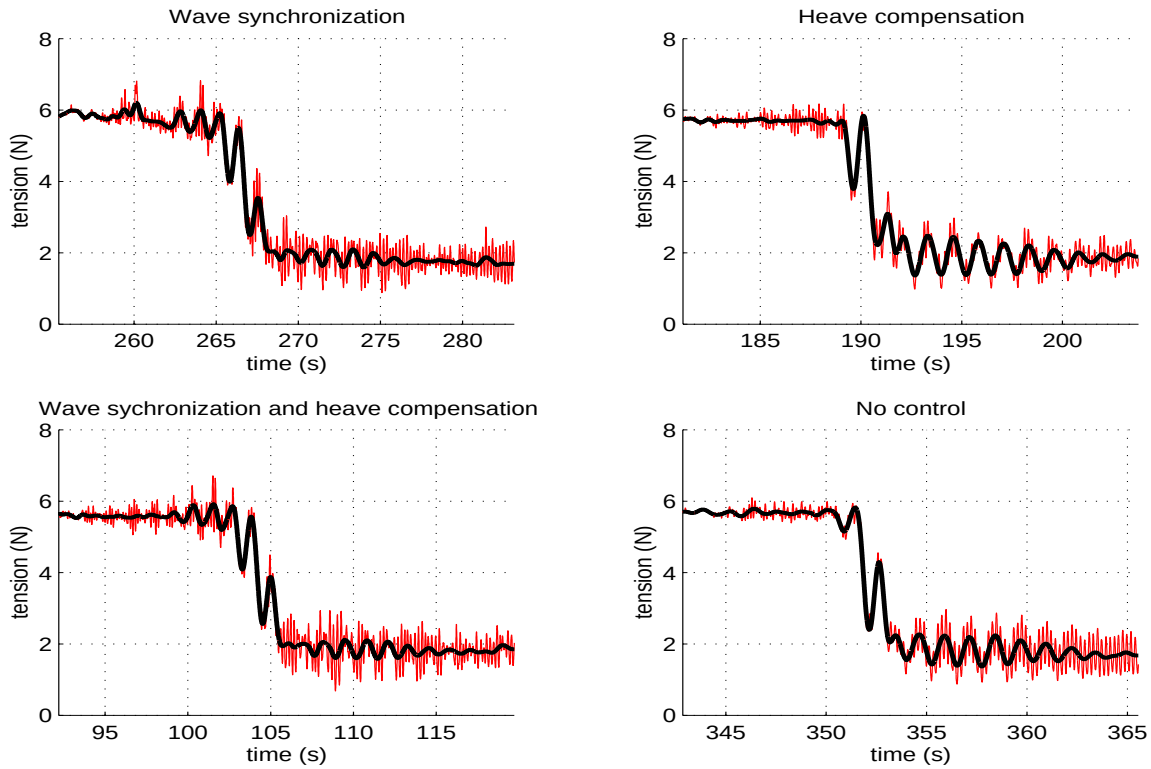

Figure 4: Experimental results with regular waves at $T = 1.25$ s and $A = 1.8$ cm, spherical payload, test B. For the wire tension we show both raw data (thin lines) and low-pass filtered data (thick lines).

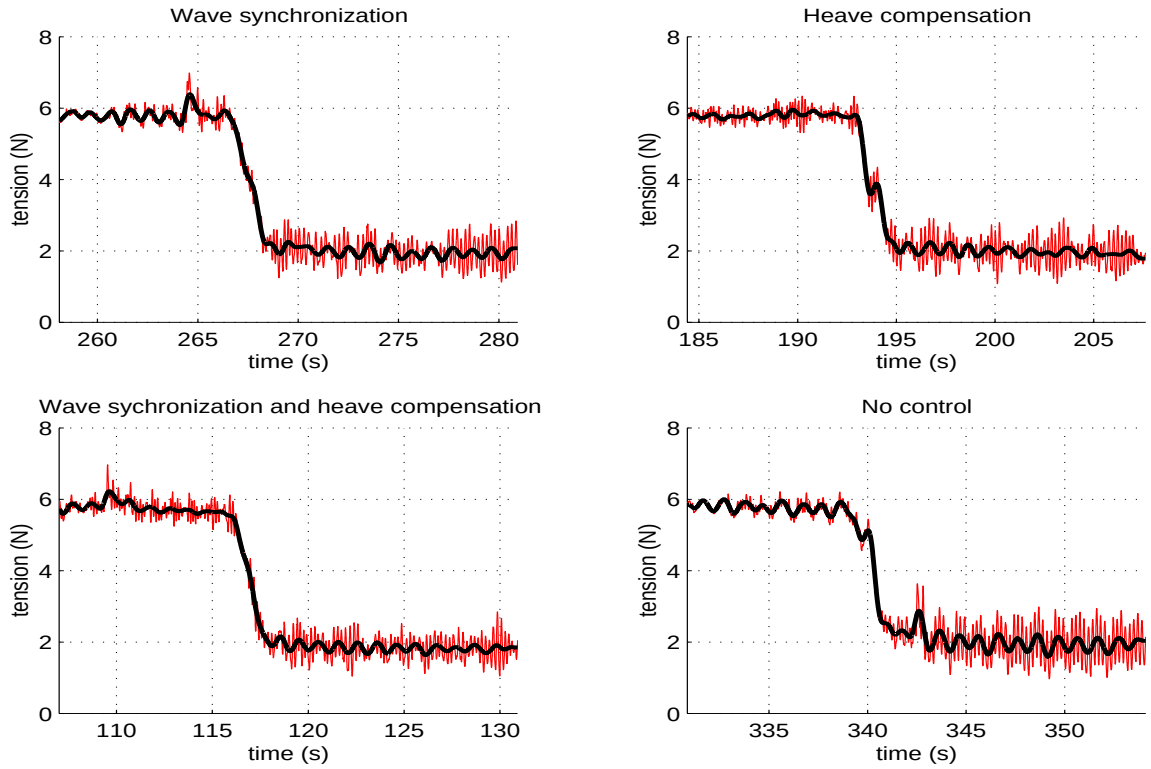

Figure 5: Experimental results with regular waves at $T = 1.00$ s and $A = 6.8$ cm, spherical payload, test B. For the wire tension we show both raw data (thin lines) and low-pass filtered data (thick lines).